Unsteady two-dimensional theory of a flapping wing

F. O. Minotti
Instituto de Física del Plasma, INFIP-CONICET, Departamento de Física, Universidad de Buenos Aires, 1428 Buenos Aires, Argentina
(Received 15 April 2002; revised manuscript received 27 August 2002; published 13 November 2002)

An analytical evaluation of the hydrodynamic force on a single flapping wing is presented, based on the two-dimensional inviscid theory, with the addition of an attached leading-edge vortex. The explicit expression of the force is given and compared with some of the measurements by Dickinson *et al.* [Science **284**, 1954 (1999)] and Sane and Dickinson [J. Expl. Biol. **204**, 2607 (2001)] for a fruit fly model wing.

DOI: 10.1103/PhysRevE.66.051907 PACS number(s): 87.10.+e, 87.19.St

I. INTRODUCTION

The fluid mechanics of insect flight has a rich and most interesting history [1]. Among other things, its study has helped to discover sophisticated mechanisms for lift generation as that of Weis-Fogh [2,3] and the pairing of downward-moving two-dimensional vortices [4]. Apart from its biological interest, the understanding of the details of insect flight has also technological interest, for instance, for the development of flying microvehicles [5]. In particular, of considerable importance are the mechanisms associated to hovering at a fixed position. For some insects such as small wasps, hovering seems to depend strongly on the interaction of two wings, as in the Weis-Fogh mechanism [2]. For many other insects, however, single wing effects are the most important, the ones to be considered in what follows. In the past few years detailed experiments with scaled insect model wings were performed, in which a careful determination was made of forces resulting from imposed complex movements [6,7]. As the relation of wing span to chord length is generally large, and the Reynolds numbers involved in the flight of most insects are of the order of a few hundreds, two-dimensional thin airfoil theory could be used, in principle, to calculate those forces. However, if steady two-dimensional aerodynamics is applied, the results are shown to underestimate the measurements. The difference is attributed basically to four mechanisms: (i) enhancement of reachable steady lift by the absence of stall, (ii) additional circulation generated by rotation of the wing, called rotational circulation, (iii) reuse, at the end of each half stroke of the wing, of previously shed vorticity, an effect known as ''wake capture,'' and (iv) the effect of added mass. The absence of stall (i), sometimes called ''delayed stall,'' is associated to the stabilization of the vorticity shed at the leading edge, thus preventing the formation of a two-dimensional von Kármán street, which ultimately destabilizes and leads to stall. As a result, a quasi-stationary, spanwise elongated vortex structure is formed near the leading edge [8]. This vortex was shown, using potential two-dimensional theory, to also produce enhanced lift with respect to the case with no vortex [9]. The stabilization of the leading-edge vortex is attributed to the spanwise flow that removes leading-edge excess vorticity from its core [8]. Recent experiments indicate that at the Reynolds numbers characteristic of insect flight a downward flow induced by tip vortices and wake vorticity can also explain the vortex stability [10]. The existence of a relatively stationary leading vortex was also found in strictly two-dimensional simulations of flapping wings [11], in which the wing changes direction rapidly, before the vortex separates. The absence of stall can also be indirectly seen in the experiment reported in Ref. [6], where the lift and drag coefficients of the model wing at fixed angles of attack are plotted as functions of time [Figs. 2(a), 2(b) in Ref. [6]]. After the initial transient the coefficients take on practically constant values with no oscillations that would reflect the shedding of vorticity at stall.

Rotational circulation (ii) is well known and can be calculated with thin airfoil theory [12] (see also Ref. [13]). It is discussed in detail in Ref. [14], where it is related to the fact that the lift coefficient of a wing increases when the angle of attack increases with time (Kramer's effect [15]). The predictions of the theory have been confirmed by the experiments [6,7].

Wake capture (iii) acts shortly after the end of each half stroke, when the wing reverts velocity and moves into the wake previously generated. With an appropriately oriented wing, the moving fluid of the wake effectively adds to the lift. Finally, added mass effects (iv) being dependent on the acceleration, are specially important near stroke reversal when the quasisteady lift associated with the velocity is very small, and also in the stages when rotational velocity changes rapidly. All these mechanisms work together and to describe their interplay a general theory that accounts for all them is required. The purpose of this work is to show, comparing with reported experiments [6,7], that the nonstationary, two-dimensional potential theory with the simple model of a stationary (with respect to the wing) two-dimensional vortex near the leading edge reproduces well the forces acting on a flapping wing. Usual Kutta-Joukowski conditions applied at both edges of the wing determine the intensity of the mentioned vortex and of bound circulation, including rotational circulation. Added mass effects are automatically included. As a result, a final analytical expression for the force is obtained, which can be used, for instance, to study different variations of complex motions and the parameter dependence of quantities of interest. At this stage wake capture effects have not been included (they are discussed with some length in the Conclusions section), but the way the formalism is introduced facilitates the inclusion of this mechanism as well improvements over the simple model used here.

II. TWO-DIMENSIONAL THEORY

To simulate the insect wing the usual model of a thin, rigid, uncambered plate is employed [6]. The flow produced

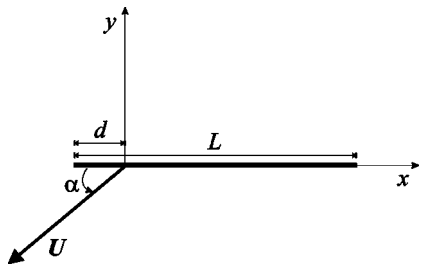

FIG. 1. Sketch showing the plate, comoving frame and conventions used.

by arbitrary two-dimensional movements of such a plate in an inviscid fluid (at rest far away) is known since many years [16]. It is presented here in a way that allows to include additional features easily, such as free or bound vortices, and also to simply evaluate the resulting hydrodynamic forces.

The plate is considered to translate with arbitrarily imposed two-dimensional velocity $\mathbf{U}(t)$ and at the same time to rotate about a fixed point contained in the plate itself with arbitrarily imposed angular velocity $\Omega(t)$, normal to the plane where the movement takes place. The goal is to evaluate the hydrodynamic force acting on the plate, taking advantage of the fact that this force is frame independent and so can be conveniently evaluated in a noninertial frame where the plate is permanently at rest. The inviscid flow in the frame where the distant fluid is at rest is irrotational (except for possible regions of concentrated vorticity, modeled as singularities of a potential flow), while the flow in the plate frame, $\mathbf{u}(\mathbf{x},t)$, has a uniform vorticity given by $-2\Omega(t)$. A Cartesian (x,y) coordinate system is taken, with the x axis along the plate's chord and the origin in the rotation axis (see Fig. 1). The incompressibility condition allows us to introduce a stream function ψ as

$$u_x=\frac{\partial\psi}{\partial y}, \quad u_y=-\frac{\partial\psi}{\partial x}. \tag{1}$$

At the same time, the flow with uniform vorticity can be decomposed into irrotational flow, of potential φ, plus a rigid body rotation:

$$u_x=\frac{\partial\varphi}{\partial x}+\Omega(t)y, \quad u_y=\frac{\partial\varphi}{\partial y}-\Omega(t)x. \tag{2}$$

Now, the modified potential and stream function are defined as

$$\tilde{\varphi}=\varphi-\Omega(t)x\,y, \quad \tilde{\psi}=\psi-\Omega(t)y^2, \tag{3}$$

which according to Eqs. (1) and (2) satisfy

$$\frac{\partial\tilde{\varphi}}{\partial x}=\frac{\partial\tilde{\psi}}{\partial y}, \quad \frac{\partial\tilde{\varphi}}{\partial y}=-\frac{\partial\tilde{\psi}}{\partial x};$$

that is, a complex potential w function can be defined with the complex variable $z=x+i\,y$ (i is the imaginary unit),

$$w(z)=\tilde{\varphi}+i\tilde{\psi}. \tag{4}$$

Since the plate is rigid and at rest in the chosen frame, its contour must coincide with a streamline, that is, the real flow in the plate's frame satisfies the boundary condition $\psi=$const over the plate ($y=0$), which, from Eq. (3), corresponds then to $\tilde{\psi}=$const at that boundary. That is, the plate corresponds to a solid boundary for the fictitious flow too. Besides, the real flow at large distances is given by

$$u_x\to -U_x(t)+\Omega(t)y,$$

$$u_y\to -U_y(t)-\Omega(t)x.$$

From Eqs. (2) and (3) it is then seen that the fictitious flow described by $w(z)$ must behave at large distances as

$$\tilde{u}_x\to -U_x(t)-\Omega(t)y,$$

$$\tilde{u}_y\to -U_y(t)-\Omega(t)x,$$

which corresponds to a complex potential given at large distances by

$$w(z)\to -U^*(t)z+\frac{i\Omega(t)}{2}z^2, \tag{5}$$

where $U(t)=U_x(t)+i\,U_y(t)$, and the asterisk denotes complex conjugation. In this way, $w(z)$ can be calculated analytically using conformal mapping methods by means of an appropriate Kutta-Joukowski transformation applied to a static circular cylinder in a flow given at large distances by the transformed version of Eq. (5). In particular, isolated singularities such as point vortices can be easily incorporated. Most importantly, it yields that the real hydrodynamic force on the plate coincides with that calculated from $w(z)$ using the Blasius formula [17]. This can be seen from the Euler equation for $\mathbf{u}(\mathbf{x},t)$ in the noninertial frame,

$$\frac{D\mathbf{u}}{Dt}=-\frac{\boldsymbol{\nabla}p}{\rho}+\mathbf{f}_r-2\boldsymbol{\Omega}\times\mathbf{u}-\frac{d\mathbf{U}}{dt}-\boldsymbol{\Omega}\times\boldsymbol{\Omega}\times\mathbf{x}-\frac{d\boldsymbol{\Omega}}{dt}\times\mathbf{x}, \tag{6}$$

where $\mathbf{f}_r$ denotes conservative real forces per unit mass, p is the pressure, ρ the constant fluid density, and D/Dt represents the material derivative. Using expressions (2) for $\mathbf{u}$, and the first of Eqs. (3), a direct replacement in Eq. (6) and a little algebra leads to a Bernoulli first integral of the Euler equation that gives (leaving out an integration constant)

$$-\frac{p}{\rho}=\frac{\partial\tilde{\varphi}}{\partial t}+\frac{1}{2}|\boldsymbol{\nabla}\tilde{\varphi}|^2+\phi_m+2\Omega(t)y\frac{\partial\tilde{\varphi}}{\partial x}, \tag{7}$$

where ϕ_m is a modified potential that includes that of the real forces ϕ_r, plus that corresponding to the conservative part of the inertial forces, and all other $\tilde{\varphi}$-independent terms with explicit spatial dependence,

$$\phi_m=\phi_r+\mathbf{x}\cdot\frac{d\mathbf{U}}{dt}-\frac{1}{2}\Omega^2(x^2+y^2)+\frac{d\Omega}{dt}xy+2\Omega^2y^2.$$

The hydrodynamic force (per unit length) over the plate is then calculated as the integral, extended along the perimeter of the plate,

$$\mathbf{F}=-\oint p\mathbf{n}dl, \tag{8}$$

where $\mathbf{n}$ is the normal to the plate and p is given by Eq. (7). In particular, the term with ϕ_m gives the Archimedes force, which is zero in the case of an infinitesimally thin plate. Besides, when evaluated over the plate ($y=0$), the last term in Eq. (7) is zero, at least for finite values of $\tilde{u}_x$ at the plate. This last condition is assured if care is taken to regularize the velocity at *both* edges of the plate. The remaining terms are precisely those considered in the derivation of the Blasius theorem (see the Appendix for a short derivation), which is applicable because the plate is at rest in the frame in which $\tilde{\varphi}$ is defined. In this way, the (complex) force per unit length can be calculated from the Blasius expression for the potential (4) as

$$F_x-iF_y=\frac{i\rho}{2}\oint\left(\frac{dw}{dz}\right)^2dz+i\rho\frac{\partial}{\partial t}\left[\oint wdz\right]^*. \tag{9}$$

III. APPLICATION

An uncambered, infinitesimally thin plate with chord length L is considered. The x axis runs along the chord, with its origin in the rotation axis which is located on the plate itself at a distance d from the leading edge (see Fig. 1). The plate boundary in the complex z plane corresponds to a circular cylinder of radius $a=L/4$ centered in the origin of the ς plane through the Kutta-Joukowski transformation [18]

$$z(\varsigma)=x_0+\varsigma+\frac{a^2}{\varsigma}, \tag{10}$$

where $x_0=L/2-d$ is (minus) the position of the rotation axis as measured from the midpoint of the plate. From Eq. (5), the complex potential in the ς plane, $\omega(\varsigma)=w[z(\varsigma)]$, is given at large distances by

$$\omega(\varsigma)\to-U^*(t)\varsigma+\frac{i\Omega(t)}{2}(\varsigma+x_0)^2, \tag{11}$$

where the x_0 in the second term must be retained, for it gives rise to a term of the same order as the first one. Applying the Milne-Thomson circle theorem [18] to Eq. (11), the transformed potential is obtained, eventually with the addition of bound circulation. Moreover, if localized singularities are needed, they can be directly incorporated in Eq. (11) prior to the application of the Milne-Thomson theorem. The force is then simply calculated by usual techniques using Eq. (9). As an example, the case of a purely rotating plate with bound circulation Γ is considered. The corresponding transformed potential is

$$\omega(\varsigma)=\frac{i\Omega(t)}{2}(\varsigma+x_0)^2-\frac{i\Omega(t)}{2}\left(\frac{a^2}{\varsigma}+x_0\right)^2+\frac{\Gamma}{2\pi i}\ln(\varsigma),$$

from which the velocity field is

$$u_x-i\,u_y=\frac{dw}{dz}=\frac{d\omega}{d\varsigma}\left(\frac{dz}{d\varsigma}\right)^{-1}=\frac{d\omega}{d\varsigma}\frac{\varsigma^2}{\varsigma^2-a^2}.$$

If the Kutta-Joukowski condition is imposed at the trailing edge (conventionally taken as that corresponding to $\varsigma=a$),

$$\frac{d\omega}{d\varsigma}\Big|_{\varsigma=a}=0,$$

the resulting circulation Γ is

$$\Gamma=4\pi a^2\Omega(t)\left(1+\frac{x_0}{a}\right)=\pi L^2\Omega(t)\left(\frac{3}{4}-\frac{d}{L}\right),$$

a well known result [12] that was experimentally verified in Refs. [6,7].

The model considered for an arbitrarily moving plate includes bound circulation Γ and also a stationary (with respect to the plate) leading-edge vortex with circulation Γ_l. Taking as b the fixed position of this vortex in the ς plane, the transformed potential can be written as

$$\begin{aligned}\omega(\varsigma)=&-U^*(t)\varsigma-U(t)\frac{a^2}{\varsigma}+\frac{i\Omega(t)}{2}(\varsigma+x_0)^2\\&-\frac{i\Omega(t)}{2}\left(\frac{a^2}{\varsigma}+x_0\right)^2+\frac{\Gamma_l}{2\pi i}\ln(\varsigma-b)\\&-\frac{\Gamma_l}{2\pi i}\ln\left(\varsigma-\frac{a^2}{b^*}\right)+\frac{\Gamma+\Gamma_l}{2\pi i}\ln(\varsigma).\end{aligned} \tag{12}$$

To regularize the velocity at both edges, the Kutta-Joukowski condition must be imposed at $\zeta=a$ and $\zeta=-a$:

$$\frac{d\omega}{d\varsigma}\Big|_{\varsigma=\pm a}=0,$$

which determines both Γ and Γ_l. The resulting expressions are, setting $b=a(\beta_x+i\beta_y)$,

$$\Gamma=\frac{4\pi a(1+\beta_x^2+\beta_y^2)(U_y+\Omega x_0)}{\beta_x(\beta_x^2+\beta_y^2-1)}+4\pi a^2\Omega, \tag{13}$$

$$\begin{aligned}\Gamma_l=&-2\pi a\beta_x^{-1}(\beta_x^2+\beta_y^2-1)^{-1}(U_y+\Omega\,x_0)[\beta_x^4+2\beta_x^2(\beta_y^2\\&-1)+(\beta_y^2+1)^2].\end{aligned} \tag{14}$$

Using Eq. (9) the force is also readily evaluated using

$$\oint\left(\frac{dw}{dz}\right)^2dz=\oint\left(\frac{d\omega}{d\varsigma}\right)^2\left(\frac{dz}{d\varsigma}\right)^{-1}d\varsigma, \tag{15a}$$

$$\oint w(z)dz=\oint\omega(\varsigma)\frac{dz}{d\varsigma}d\varsigma, \tag{15b}$$

and considering as internal singularities those located at $\varsigma=0$, $\varsigma=-a$ (if this is taken to correspond to the leading

edge; the resulting force is independent of this choice), and $\varsigma = a^2/b^*$. The integral in Eq. (15a) is easily performed by residues, as the terms in Eq. (15b) with no logarithmic dependence, while the rest of the terms can be evaluated readily taking care of the logarithm branch cut. As a result of the regularization of the velocity at both edges, the force is normal to the plate ($F_x = 0$). The y component of the force is given by the sum of the two following expressions, again with $b = a(\beta_x + i\beta_y)$:

$$F_y^{(a)} = 4\pi a\rho\beta_x^{-2}(\beta_x^2+\beta_y^2)^{-1}(\beta_x^2+\beta_y^2-1)^{-3}\{U_x\beta_x(\beta_x^2 + \beta_y^2)(\beta_x^2+\beta_y^2-1)^2[U_y(1-\beta_x^2+\beta_y^2)+\Omega(x_0-a\beta_x - x_0\beta_x^2+a\beta_x^3+x_0\beta_y^2+a\beta_x\beta_y^2)]+(U_y+\Omega x_0)^2\beta_y \times[-\beta_x^8-2\beta_x^6(\beta_y^2-1)+\beta_y^4(\beta_y^2+1)^2+2\beta_x^2\beta_y^4(\beta_y^2 + 3)+\beta_x^4(6\beta_y^2-1)]+a\Omega(U_y+\Omega x_0)\beta_y[\beta_x^9 + 4\beta_x^7(\beta_y^2-1)+\beta_x(\beta_y^4-1)^2+2\beta_x^5(3\beta_y^4-4\beta_y^2+3) + 4\beta_x^3(\beta_y^6-\beta_y^4+\beta_y^2-1)]\}, \quad (16)$$

$$F_y^{(b)} = -2a\rho\left\{\frac{d\Gamma}{dt}+\frac{d\Gamma_l}{dt}\left[1+\frac{\beta_x}{\beta_x^2+\beta_y^2}(1-\sqrt{\beta_x^2+\beta_y^2})\right]\right\} - 4\pi a^2\rho\left(\frac{dU_y}{dt}+x_0\frac{d\Omega}{dt}\right), \quad (17)$$

where $F_y^{(a)}$ comes from the integral (15a), and $F_y^{(b)}$ from Eq. (15b).

At this point an important issue needs to be discussed. In the potential proposed, Eq. (12), no representation exists of the vorticity shed by the plate to adjust the circulation Γ so as to fulfill the Kutta-Joukowski condition when U and Ω change. In principle, a trailing vortex sheet should be present to account for this shed vorticity, which is ultimately swept away. Analogously, a vortex sheet should also exist at the leading edge, to feed vorticity to the leading vortex. The force generated by these sheets is not considered in the model, for the vorticity content in them is not expected to be important at any given time, and that vorticity is either swept away or included in the leading vortex. However, they play a key role in the determination of the precise way in which the circulation adjusts to changes in the velocities of the wing [19]. In this way, the vortex sheets have an indirect effect on the force through the values of $d\Gamma/dt$ and $d\Gamma_l/dt$ in Eq. (17) that they determine. To estimate this effect we use the results in Ref. [19] where the shedding of vorticity and generation of circulation on unsteady airfoils is studied in detail for starting flows. In particular, it is determined in that Ref. [19] that a starting flow in which $U_x \sim t^\gamma$, $U_y \sim t^\gamma$ generates a circulation over an airfoil with a cusplike trailing edge that behaves to leading order in t as $\Gamma \sim t^\mu$, with $\mu = (3\gamma+1)/2$ or $\mu = (4\gamma+1)/3$, depending on whether the convection of the vortex sheet is dominated by U_x or U_y, respectively. For a velocity field with finite time derivative at $t=0$, that is, $\gamma = 1$, the circulation then grows very slowly, as $\Gamma \sim t^2$ or $\Gamma \sim t^{5/3}$; in particular, $d\Gamma/dt = 0$ at $t=0$, when $d\mathbf{U}/dt$ is finite. This result applies, of course, also to the change in circulation from a constant, finite value, when the velocity of the wing changes at $t=0$, and shows that taking into account the dynamics of the shed vorticity results in much smaller values of $d\Gamma/dt$ than those corresponding to assuming the instantaneous adjustment of the circulation to the changing conditions of the flow (this is reminiscent of the Wagner effect for impulsively started wings [20]). A simple possible way of including the effect considered is to take $d\Gamma/dt = d\Gamma_l/dt = 0$ in the evaluation of the last term in Eq. (17), while still assuming the instantaneous adjustment of Γ for the rest of the terms, which could be termed a quasistationary approach.

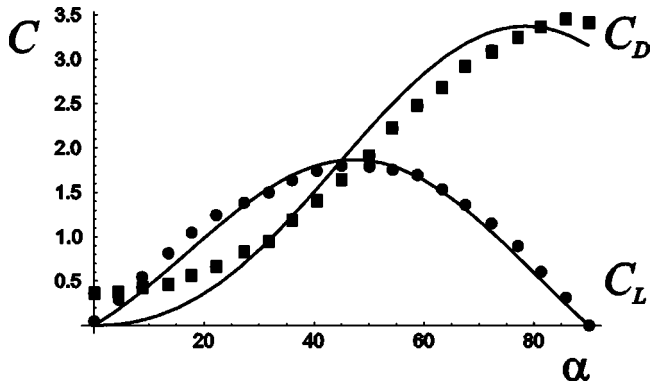

FIG. 2. Coefficients of lift (C_L) and drag (C_D) for the model wing, as obtained from the theory with $b/a = -1.25 + i\,0.48$, solid line, and experimental values from Ref. [6], dots and squares.

A complementary justification of this choice comes from the following. For a body with time dependent bound circulation Γ, the force term proportional to $d\Gamma/dt$, by itself, is not physically correct, in general. For instance, in the case of a stationary cylinder of radius a and circulation Γ, a change in Γ would give rise to a finite force ($F_x = 0, F_y = -\rho a\, d\Gamma/dt$) violating isotropy in the (x,y) plane. Similarly, for a thin airfoil the corresponding term is easily seen to violate reflection symmetry. The only value that gives acceptable forces at this level of approximation is $d\Gamma/dt = 0$.

With these considerations the condition $d\Gamma/dt = d\Gamma_l/dt = 0$ will be used in Eq. (17); however, since this approximation yields the full time derivatives, it will also be presented for comparison purposes.

There exists still an explicit dependence on the parameter b, which reflects the three-dimensional nature of the problem, as the stabilization of the leading-edge vortex is a genuine three-dimensional effect (see Refs. [8,10]). In the present model b is determined so as to adjust the experimental lift and drag coefficients reported in Ref. [6] for all angles of attack. In Fig. 2 the results obtained with $b = a(-1.25 + i\,0.48)$ are presented, together with the experimental values. The following definitions for the lift and drag coefficients, respectively, were used

$$C_L = \frac{2F_y\cos\alpha}{\rho|\mathbf{U}|^2 L}, C_D = \frac{2F_y\sin\alpha}{\rho|\mathbf{U}|^2 L},$$

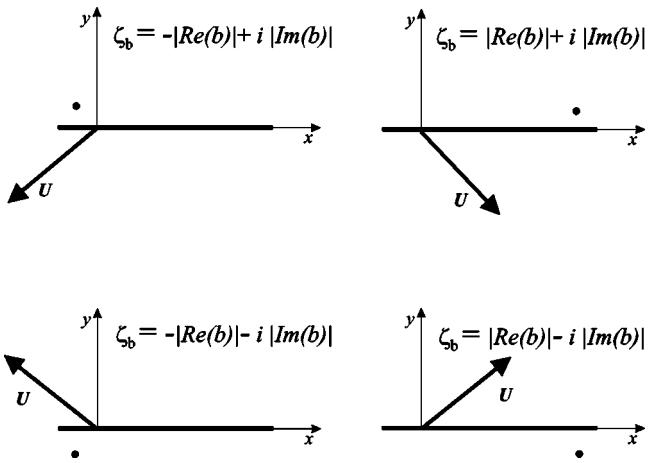

FIG. 3. Schematic position of the leading vortex, represented by the dot, according to the different orientations of velocity, together with the corresponding coordinates in the ς plane.

with α the angle of attack. The experiments were performed under stationary conditions, so in Eq. (16) one must take $\Omega=0$ and $\mathbf{U}=\text{const}$, with $U_x=-|\mathbf{U}|\cos\alpha$ and $U_y=-|\mathbf{U}|\sin\alpha$.

Of course, the theory does not reproduce the small viscous drag that gives a nonzero drag coefficient for zero angle of attack, but the overall agreement is rather good, considering that a single value of b was used.

For complex movements of the wing the same position for the vortex, relative to the leading edge, is assumed, which is only an approximation, expecting that the adjustment of only the circulation Γ_l may compensate for possible changes in b.

A related final consideration is that care must be taken to choose the leading edge as that for which the angle with the velocity vector is acute. In this way, the value of b must be changed to keep the relative position fixed. This is required when the angle of attack crosses 90° or when the velocity reverts, and reduces simply to changing appropriately the sign of the real and/or imaginary part of b, as shown in Fig. 3, which can be simply expressed as

$$\zeta_b=|\mathrm{Re}(b)|\,\mathrm{sgn}(U_x)-i|\mathrm{Im}(b)|\,\mathrm{sgn}(U_y). \qquad (18)$$

This is in fact a very simple modelization of the detachment of the leading vortex and its replacement by a newly generated one at a different position.

IV. RESULTS

In the experiments to be analyzed, the motion of the model wing is genuinely three-dimensional as the velocity changes along the wing length (the wing tip describes a spherical motion), so that the application of a two-dimensional theory requires some elaboration. The usual approach is the blade element method (see Ref. [14]) that results in expressions for the hydrodynamic force depending on different averages over the wing length. In this work a simpler approach will be adopted: the velocity used to evaluate the force is taken as the wing tip velocity times the square root of the nondimensional second moment of the wing area. This is the correct result of the blade element theory for a rotating wing at constant angular velocity and fixed angle of attack, and seems to be a reasonable good approximation for the more complex cases considered.

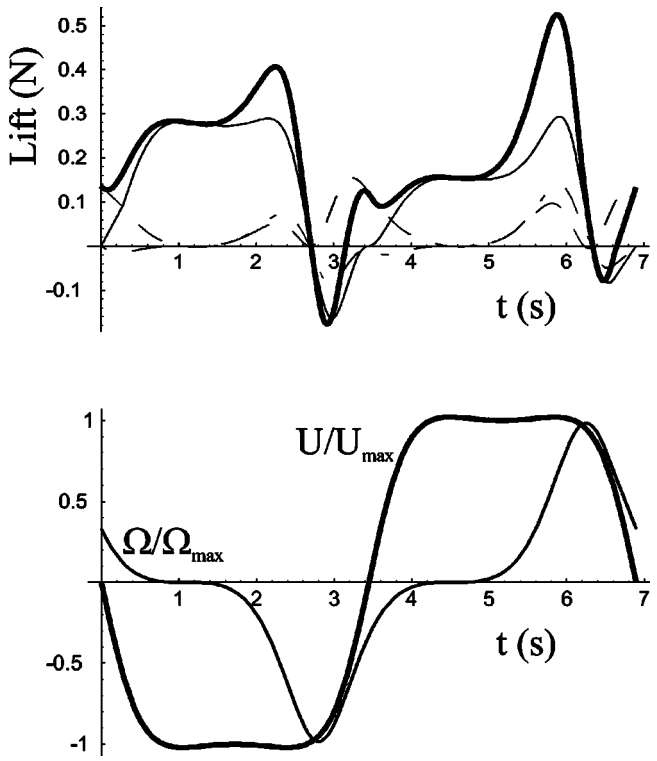

FIG. 4. Upper panel: theoretical lift force (thick solid line) during a flapping cycle and its different contributions—translational lift (thin solid line), rotational lift (short dashes) and added mass (long dashes). Lower panel: translational and rotational velocities during the flapping cycle. $U_{\max}=14.5$ cm s^{-1}, $\Omega_{\max}=1.96$ s^{-1}.

The experimental results are simulated using a chord length $L=6.5$ cm, wing length $L_W=25$ cm, and distance between leading edge and rotation axis, $d=0.25L$, deduced from data in Refs. [6,7]; the density of the oil used in the experiment is $\rho=0.88$ g cm^{-3}. In the lower panel of Fig. 4 are represented the profiles of translational and rotational velocities emulating the wing movement of the fruit fly model [6], where $U_{\max}=14.5$ cm s^{-1}, and $\Omega_{\max}=1.96$ s^{-1}. The velocity was taken to be always horizontal, which is well satisfied in the experiment, and represented by the expression

$$U(t)=-U_{\max}\frac{(1+c_1)\sin(\omega t)}{1+c_1\sin^2(\omega t)},$$

where the flapping angular frequency is $\omega=2\pi\times 145$ mHz, and $c_1=1.5$ reproduces well the experimental profile. The value of $U_{\max}$ corresponds to an averaged value over the wing length, given by $U_{\max}=U_0\sqrt{\hat{r}_2^2}$, where $\hat{r}_2^2=0.4$ is the nondimensional second moment of the wing area, and $U_0=23$ cm s^{-1} is the maximum velocity of the wing tip.

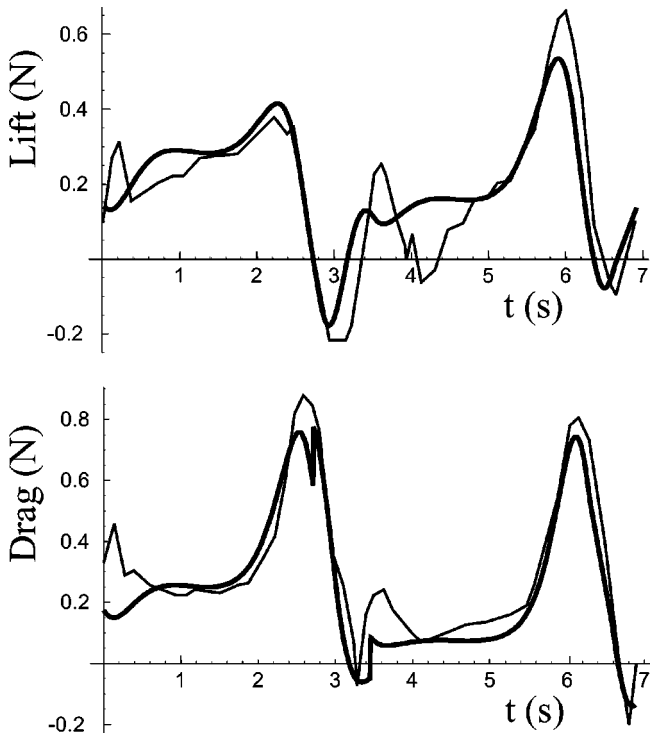

FIG. 5. Theoretical (thick solid line) and experimental (thin solid line) force during a flapping cycle with the time derivative of circulations equal to zero. Upper panel: lift force. Lower panel: drag force.

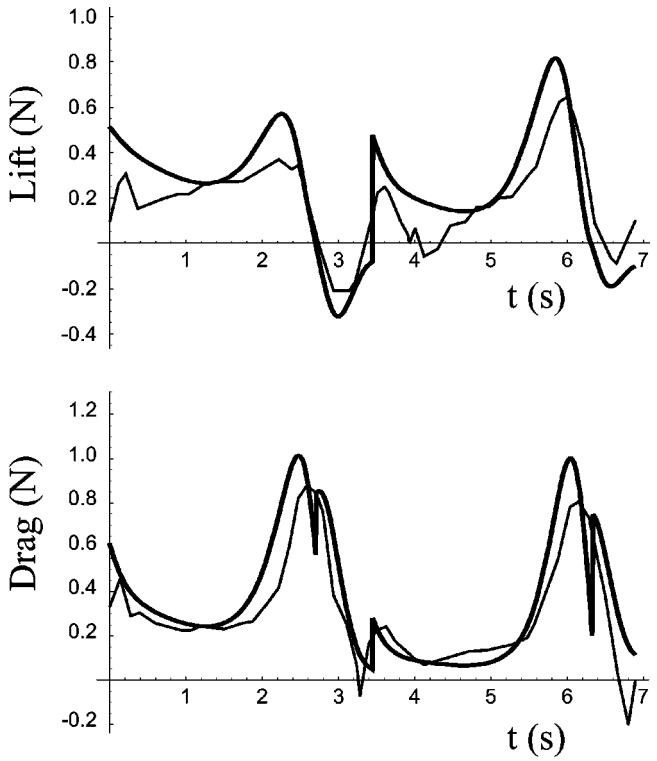

FIG. 6. Theoretical (thick solid line) and experimental (thin solid line) force during a flapping cycle with the time derivative of circulations included. Upper panel: lift force. Lower panel: drag force.

The angle of attack was represented by a similar expression

$$\alpha(t)=\alpha_0+\alpha_1\left[\frac{(1+c_2)\sin(\omega t-\theta)}{1+c_2\sin^2(\omega t-\theta)}+\frac{(1+c_2)\sin(\theta)}{1+c_2\sin^2(\theta)}\right],$$

with $c_2=1$, and $\theta=0.8125\pi$. The values of α_0 and α_1 were chosen to satisfy the experimental conditions $\alpha=40°$ in the middle of the downstroke ($t=0.5\pi/\omega$), and $\alpha=180°-20°$ at the middle of the upstroke ($t=1.5\pi/\omega$), resulting in $\alpha_0=49°$ and $\alpha_1=60°$. The angular velocity is then given by

$$\Omega(t)=-\frac{\pi}{180}\frac{d\alpha}{dt},$$

resulting in the above reported value of $\Omega_{\max}$.

In the upper panel of Fig. 4 the different contributions to theoretical total lift (thick solid line) are shown. They correspond to purely translational lift, which is calculated as the force given by Eq. (16) with $\Omega=0$; the rotational lift calculated as the difference between Eq. (16) and the translational contribution; and the added mass contribution Eq. (17) with $d\Gamma/dt=d\Gamma_l/dt=0$. As can be seen, rotational and added mass contributions are of similar importance and both add up to produce the strong peaks that increase the lift over the purely translational component.

In Fig. 5 the theoretical lift and drag forces are shown, together with the reported experimental values for the choice $d\Gamma/dt=d\Gamma_l/dt=0$. The main features are reasonably well reproduced both in phase and magnitude. The peaks occurring in both forces near $t=0.2$ s and $t=3.6$ s, which are not reproduced by the model, are probably due to wake capture effects, as both take place ≈ 0.2 s s after stroke reversal, which occurs at $t=0$ and at $t=3.4$ s. The same kind of effect is probably responsible too for the valleys following both peaks, also not reproduced by the theoretical results.

The two dips near the peaks of theoretical drag coincide with the angle of attack crossing 90°, and are the result of the corresponding change in position of the leading vortex from one edge of the plate to the other (see Fig. 3); since at that moment the angular velocity is nonzero (it is almost at its peak) there is a small discontinuity in the drag force revealed by the dip (for $\Omega=0$, by reflection symmetry, at an angle of attack of 90° the force does not depend on which edge the leading vortex is attached to, and no discontinuity shows up).

The effect of considering the time derivatives of Γ and Γ_l in Eq. (17) is shown in Fig. 6, where the corresponding theoretical lift and drag forces are shown, together with the experimental values. The comparison with Fig. 5 indicates that the main features of the force are also reasonably well reproduced. In particular, the peaks missing in Fig. 5 show up here, generated by the new terms, which are also responsible for the increased values of the other peaks. Although it is tempting to consider the new terms genuinely responsible for the observed peaks near $t=0.2$ s and $t=3.6$ s, for the arguments given above it is more probable that they are due to wake capture effects, and that the new terms spuriously

overestimate nonstationary effects.

Finally, a comparison was made with some of the results reported in Ref. [7]. There, a wide variety of flapping patterns are presented, among which those with the most complex structure were chosen for comparison purposes. They correspond to the ''oval'' and ''figure of eight'' patterns determined by the superposition of the horizontal and vertical (or meridional) motion of the wing.

Again, a more correct application of a two-dimensional theory to a genuine three-dimensional motion would result in very involved expressions, specially for the complex patterns considered. To obtain a simpler approximation, corrections to the radius of horizontal rotation and other vector projections due to stroke deviation from the mean stroke plane will be neglected (they represent factors in the range $[\sim 0.9,1]$ in the patterns analyzed). Similarly, the angle α will be taken to correspond to the angle between wing chord and mean stroke plane. All these approximations become exact in the limit of horizontal motion and are expected to give good results for the small angles ($\leqslant 25°$) of stroke deviation in the patterns shown.

In this way, to simulate the tip velocities in the experiment the following expressions are used for the horizontal and vertical motion, respectively:

$$U_H(t) = U_{H0} \frac{\tanh[c_1 \sin(\omega_H t)]}{\tanh(c_1)}, \tag{19a}$$

$$U_V(y) = U_{V0} \cos(\omega_V t), \tag{19b}$$

where $\omega_H = 2\pi \times 170$ mHz, $c_1 = 4.762$, $\omega_V = \omega_H$ for the oval pattern and $\omega_V = 2\omega_H$ for the figure of eight pattern, $\Theta(t)$ is the angle between the axis of the wing and the horizontal plane $\Theta(t) = \Theta_0 \sin(\omega_V t)$, with Θ_0 being the vertical angular amplitude. The velocity amplitudes are $U_{H0} = L_W \Phi_0 \omega_H / \pi$ and $U_{V0} = L_W \Theta_0 \omega_H$, with L_W being the wing length and Φ_0 the peak-to-peak-amplitude of horizontal angular motion. The angle between wing chord and the horizontal plane is given by

$$\alpha(t) = \frac{\pi}{2} + \left(\alpha_0 - \frac{\pi}{2} \right) \frac{\tanh\{c_2 \sin[\omega_H (t + t_0)]\}}{\tanh(c_2)},$$

where $\alpha_0 = 45\pi/180$, $c_2 = 4.762$, and $t_0 = 0.2941$. The angular velocity is given by $\Omega(t) = -d\alpha/dt$. In the patterns presented $\Phi_0 = \pi$ and $\Theta_0 = \pm 25\pi/180$, where the positive (negative) value corresponds to upward (downward) motion at the beginning of downstroke. The values of c_1 and c_2 were chosen so that the flip duration of both U_H and α lasts $0.1T$, with $T = 2\pi/\omega_H$. The value of t_0 corresponds to α starting a flip at time $0.1T$ before stroke reversal. The values of wing parameters and ambient fluid were taken to be the same in both experiments and the velocities in Eq. (19) were multiplied by $\sqrt{\hat{r}_2^2}$, again with $\hat{r}_2^2 = 0.4$, to be used as averaged values in Eqs. (16) and (17). Lift and drag are defined following the convention used in Ref. [7]. The results for $d\Gamma/dt = d\Gamma_l/dt = 0$ are shown in Fig. 7 together with the experimental values. *A* and *B* correspond to the oval pattern, while *C* and *D* to the figure of eight pattern, differing in each case in the direction of vertical motion at the beginning of downstroke.

As indicated in Ref. [7] the upstroke of case *A* (second half period) and the downstroke of case *B* (first half period) are characterized by substantial wake effects at the start of the stroke, which can explain the differences between experimental and theoretical results in those parts of the strokes. The systematic underestimation of the theoretical force during most of the upstroke in case *A*, not seen in case *B*, is particularly interesting. This may be an indication of a more persistent wake capture due to the downward motion of the wing. The forces in the figure of eight patterns with their expected more complex wing-wake interaction are less well represented by the theory. Some of the differences can be attributed to the approximate representation of the velocity and angle as functions of time used in the theoretical description. Since the force depends on second-order time derivatives of angle (and first order of velocity) it is very sensitive to the details of the motion. In fact, slight changes in the parameters of the motion, such as flip duration and flip time, lead to marked changes in the forces. In order for this to be appreciated and to facilitate the use of the formalism for other cases, an annotated and easy to use MATLAB script was written to simulate all possible patterns (with the approximations mentioned above) in the experiment [21].

V. CONCLUSIONS

The nonstationary two-dimensional potential theory to model the forces on a flapping wing was developed. The theory allows analytical computations and the modelization of different mechanisms of importance. In particular, the rather crude model of a stationary vortex, which ensures regularization of the velocity at the leading edge, reproduces with reasonable accuracy the measured forces, and has the advantage of leading to an explicit general expression for the force. There remains the point of whether different values of the position of the mentioned vortex, represented by the value of b in Eq. (16), are needed to model different wing shapes. In principle, since the mechanisms that stabilize the leading vortex seem to be of a three-dimensional nature, it is reasonable to suppose that there should be a dependence on the wing shape. On the other hand, the two-dimensional direct numerical simulations performed in Ref. [11] give values for the lift coefficient similar to those in Fig. 2 when the thickness of the simulated wing tends to zero. This could be an indication of a more general validity of the value used for b.

A particularly important point is the consideration of the zero time derivative for the circulations in Eq. (17). It was argued that if vortex sheets conveying the shed vorticity were included, the circulations would have smaller time derivatives than those resulting from an approximation that does not include those sheets, and that the simplest, physically acceptable model corresponds to zero time derivatives. The simple comparison of the results with zero and nonzero time derivatives does not decisively favor either of them, and in this respect it would be of much interest to perform ex-

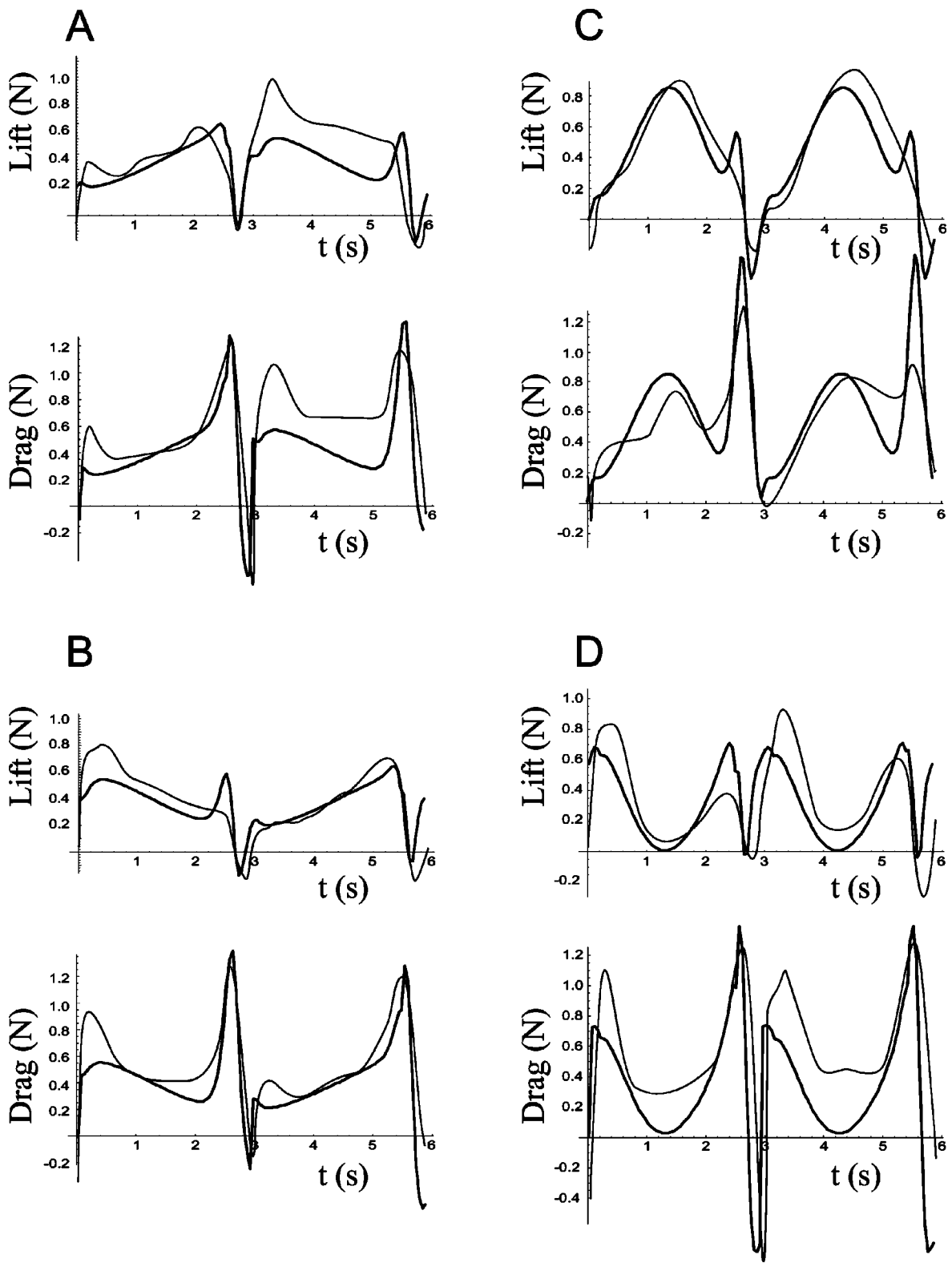

FIG. 7. Theoretical (thick solid line) and experimental (thin solid line) lift and drag forces for different flapping patterns, with zero time derivative of circulations. (a) Oval pattern with upward motion at beginning of downstroke. (b) Oval pattern with downward motion at beginning of downstroke. (c) Figure of eight pattern with upward motion at beginning of downstroke. (d) Figure of eight pattern with downward motion at beginning of downstroke.

periments in which a more decisive comparison can be made; for instance, an experiment in which wake capture effects were minimized, such as a flapping with simultaneous fast translation.

Finally, a few considerations can be made about the effect of wake capture. At the end of a half stroke, when $\mathbf{U}\to 0$ and Ω has a value Ω_0, the magnitude of the leading vortex is given by expression (14) to be (for the value of b used) $\Gamma_l \simeq 9.8 x_0 a \Omega_0 \simeq 1.2 L^2 \Omega_0$. This vortex is the one that during the time it stays close to the plate produces the additional force. A more complete theory should take into consideration its subsequent movement and interaction with the wing. At this point we can only make a rough estimation of the force (per unit wing span) due to this vortex (using the standard potential theory) as $F_w \approx \rho \Gamma_l^2 / L \approx \rho L^3 \Omega_0^2$, which can be compared, for instance, to the maximum translational component, estimated as $F_t \approx \rho L U_{\max}^2$. In this way, we could anticipate strong wake capture effects if the squared rotational velocity at stroke reversal, Ω_0^2, is not small compared to $(U_{\max}/L)^2$. In the results shown in Figs. 4 and 5 one has $(\Omega_0 L/U_{\max})^2 \simeq 0.1$, so that the formalism can be applied with some confidence. This is not the case for the hoverfly model, also considered in Ref. [6], in which it is precisely $\Omega_0 = \Omega_{\max}$, and $(\Omega_{\max} L/U_{\max})^2 \simeq 1.85$, so that wake capture effects are very notorious.

ACKNOWLEDGMENTS

The author acknowledges grants of the CONICET and of the University of Buenos Aires.

APPENDIX

A simple derivation of the Blasius formula (9) is included here to make the mathematical approach employed more self-contained. For this, consider the evaluation of Eq. (8) with only these terms of Eq. (7) that contribute to the force

$$\mathbf{F} = \rho \oint_{\mathfrak{C}} \left(\frac{1}{2} \left| \nabla \tilde{\varphi} \right|^2 + \frac{\partial \tilde{\varphi}}{\partial t} \right) \mathbf{n} dl, \tag{A1}$$

where $\mathfrak{C}$ is a curve representing the static solid boundary in the (x,y) plane, dl represents a differential length along the curve, and $\mathbf{n}$ is the (external) normal. One can then write

$$\mathbf{n} dl = d\mathbf{l} \times \mathbf{k} = dy\,\mathbf{i} - dx\,\mathbf{j}, \tag{A2}$$

where $\times$ represents the vector product, $d\mathbf{l} = dx\,\mathbf{i} + dy\,\mathbf{j}$ is the vector differential displacement along the curve, $(\mathbf{i},\mathbf{j})$ are unit vectors along the (x,y) coordinates, and $\mathbf{k}$ is the unit vector normal to the (x,y) plane. It is at this point useful to introduce the complex representation of two-dimensional vectors: $A_x\mathbf{i} + A_y\mathbf{j} \to A_x + iA_y$, which allows us to write, from Eq. (A2), $\mathbf{n} dl \to -i(dx + i dy) = -i dz$, and represent Eq. (A1) as

$$F_x + iF_y = -\frac{i\rho}{2} \oint_{\mathfrak{C}} |\nabla \tilde{\varphi}|^2 dz - i\rho \oint_{\mathfrak{C}} \frac{\partial \tilde{\varphi}}{\partial t} dz. \tag{A3}$$

Using

$$|\nabla \tilde{\varphi}|^2 = |\tilde{\mathbf{u}}|^2 = \left(\frac{dw}{dz} \right)^* \frac{dw}{dz},$$

the complex conjugate of Eq. (A3) can be written as

$$F_x - iF_y = \frac{i\rho}{2} \oint_{\mathfrak{C}} \frac{dw}{dz} \left(\frac{dw}{dz} \right)^* dz^* + i\rho \frac{\partial}{\partial t} \left(\oint_{\mathfrak{C}} \tilde{\varphi} dz \right)^*. \tag{A4}$$

The time derivative was taken out of the second integral because the solid is at rest. For the same reason, the solid boundary corresponds to a streamline and so, along the boundary, $\tilde{\psi} = \text{const}$ or $d\tilde{\psi} = 0$; that is, $dw = d\tilde{\varphi} + i d\tilde{\psi}$ is real along the boundary, which allows us to write

$$\left(\frac{dw}{dz} \right)^* dz^* \Big|_{\mathfrak{C}} = dw^* \Big|_{\mathfrak{C}} = dw \Big|_{\mathfrak{C}} = \frac{dw}{dz} dz \Big|_{\mathfrak{C}}, \tag{A5}$$

and, since $\oint_{\mathfrak{C}} dz = 0$,

$$\oint_{\mathfrak{C}} \tilde{\varphi} dz = \oint_{\mathfrak{C}} (w - i\tilde{\psi}) dz = \oint_{\mathfrak{C}} w dz. \tag{A6}$$

Replacement of Eqs. (A5) and (A6) in Eq. (A4) leads then to expression (9).

[1] T. Maxworthy, Annu. Rev. Fluid Mech. **13**, 329 (1981).
[2] T. Weis-Fogh, J. Exp. Biol. **59**, 169 (1973).
[3] M.J. Lighthill, J. Fluid Mech. **60**, 1 (1973).
[4] Z.J. Wang, Phys. Rev. Lett. **85**, 2216 (2000).
[5] C.P. Ellington, J. Exp. Biol. **202**, 3439 (1999).
[6] M.H. Dickinson, F.-O. Lehmann, and S.P. Sane, Science **284**, 1954 (1999).
[7] S.P. Sane and M.H. Dickinson, J. Exp. Biol. **204**, 2607 (2001).
[8] T. Maxworthy, J. Fluid Mech. **93**, 47 (1979).
[9] S. Savage, B.G. Newman and D.T.-M. Wong, J. Exp. Biol. **83**, 59 (1979).
[10] J.M. Birch and M.H. Dickinson, Nature (London) **412**, 729 (2001).
[11] Z.J. Wang, J. Fluid Mech. **410**, 323 (2000).
[12] Y.C. Fung, *An Introduction to the Theory of Aeroelasticity*, (Wiley, New York, 1955).
[13] C.P. Ellington, Philos. Trans. R. Soc. London, Ser. B **305**, 79 (1984).
[14] S.P. Sane and M.H. Dickinson, J. Exp. Biol. **205**, 1087 (2002).
[15] M. Kramer, Z. Flugtech. u. Motorluftschif. **23**, 185 (1932).
[16] We were able to trace it back to 1917 in V. Valcovici, Acad. Sci. III **165**, 147 (1917), as cited in C. Jacob, *Introduction*

Mathématique à la Mécanique des Fluides (Gauthier-Villars, Paris, 1959), p. 458.
[17] C. Jacob, *Introduction Mathématique à la Mécanique des Fluides* (Gauthier-Villars, Paris, 1959).
[18] G.K. Batchelor, *An Introduction to Fluid Dynamics* (Cambridge University Press, 2000).
[19] J.M.R. Graham, J. Fluid Mech. **133**, 413 (1983).
[20] H. Wagner, Z. Angew. Math. Mech. **5**, 17 (1921).
[21] This script called ''fly.m'' can be downloaded from http://www/lfp.uba.ar and used as it stands or modified for other applications.